Weierstraß-Institut
für Angewandte Analysis und Stochastik
Leibniz-Institut im Forschungsverbund Berlin e. V.

Hybrid mode-locking in edge-emitting semiconductor lasers: Simulations, analysis and experiments

Rostislav Arkhipov[1], Alexander Pimenov[1], Mindaugas Radziunas[1],

Andrei G. Vladimirov[1], Dejan Arsenjević[2], Dmitrii Rachinskii[3],

Holger Schmeckebier[2], Dieter Bimberg[2]

submitted: September 17, 2012

[1] Weierstrass Institute
    Mohrenstr. 39
    10117 Berlin, Germany
    E-Mail: Rostislav.Arkhipov@wias-berlin.de
         Aleksandr.Pimenov@wias-berlin.de
         Mindaugas.Radziunas@wias-berlin.de
         Andrei.Vladimirov@wias-berlin.de

[2] Institut für Festkörperphysik
    Technische Universität Berlin
    Hardenbergstr. 36
    10623 Berlin, Germany
    E-Mail: dejan@sol.physik.tu-berlin.de
         schmeckebier@sol.physik.tu-berlin.de
         bimberg@physik.tu-berlin.de

[3] Department of Applied Mathematics
    University College Cork
    Cork, Ireland
    E-Mail: D.Rachinskii@ucc.ie

No. 1734

Berlin 2012

Abstract

Hybrid mode-locking in a two section edge-emitting semiconductor laser is studied numerically and analytically using a set of three delay differential equations. In this set the external RF signal applied to the saturable absorber section is modeled by modulation of the carrier relaxation rate in this section. Estimation of the locking range where the pulse repetition frequency is synchronized with the frequency of the external modulation is performed numerically and the effect of the modulation shape and amplitude on this range is investigated. Asymptotic analysis of the dependence of the locking range width on the laser parameters is carried out in the limit of small signal modulation. Our numerical simulations indicate that hybrid mode-locking can be also achieved in the cases when the frequency of the external modulation is approximately twice larger and twice smaller than the pulse repetition frequency of the free running passively mode-locked laser f_P. Finally, we provide an experimental demonstration of hybrid mode-locking in a 20 GHz quantum-dot laser with the modulation frequency of the reverse bias applied to the absorber section close to $f_P/2$.

1   Introduction

Passively mode-locked (ML) semiconductor lasers are widely used for the generation of short optical pulses with repetition rates of a few to hundred GHz [1, 2]. Nowadays, a new generation of passively ML quantum dot lasers, which demonstrate a number of important advantages as compared to standard quantum well devices, such as low threshold pump current, temperature stability, low chirp of the pulses etc., become very promising for local area networks or optical clocks operating at 1.3 μm. Due to the presence of spontaneous emission and other noise sources, pulses emitted by passively ML lasers usually exhibit a considerable time jitter. An effective method for suppressing this jitter is based on hybrid mode-locking. In hybrid ML lasers the reverse bias applied to the saturable absorber (SA) section is modulated at the frequency f_M close to the pulse repetition frequency f_P of the free running passively ML laser [3, 4, 5, 6, 7, 8]. When the frequency detuning $\delta f = f_M - f_P$ becomes sufficiently small, the pulse repetition frequency synchronizes to the frequency f_M of the external modulation. The frequency range in which this synchronization takes place is usually referred to as the locking range.

Experimental studies of hybrid mode-locking in 40 GHz quantum dot laser were carried out in [6, 7, 8, 9]. In Ref. [8, 9] evolution of the locking range with the increasing reverse bias modulation amplitude has been investigated experimentally and theoretically. It was shown that the locking range increases almost linearly with the modulation amplitude and exhibits a strong asymmetry with respect to the frequency f_P of the free running passively ML laser.

In this paper we perform a theoretical analysis of hybrid mode-locking in semiconductor lasers. This analysis is based on a set of three delay differential equations (DDE) describing time evolution of the field amplitude, saturable gain, and saturable absorption. The DDE model was first derived in [10, 11, 12] for the case of unidirectional lasing in a ring cavity and Lorentzian shape of the spectral filtering element, see a schematic representation of such a laser in Fig. 1(a).
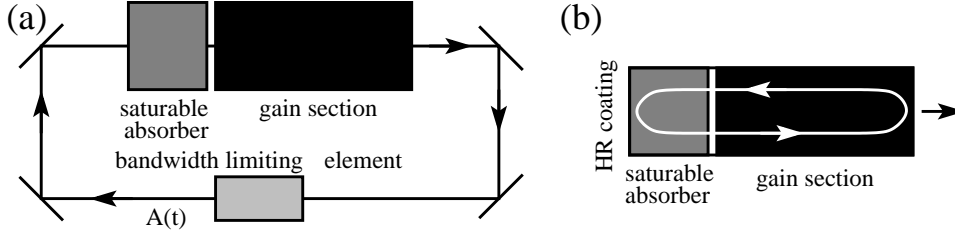
Figure 1: Schematic representation of a mode-locked laser in (a) ring and (b) linear configurations.

Later this model was extended to take into account the carrier exchange between carrier reservoir and discrete levels in quantum dots [14, 15, 8]. In this paper, however, in order to keep our numerical and analytical analysis as simple as possible, we use the original version of the DDE model proposed in [10, 11, 12].

The structure of the paper is as follows. In Section 2 we introduce the model equations for hybrid ML laser and present numerical estimates of the locking range for three different cases of harmonic modulation. In addition to the standard case, where the frequency of the external modulation is close to the pulse repetition frequency, $f_M \approx f_P$, we consider modulations of twice higher frequency, $f_M \approx 2f_P$, [second harmonic (SH) modulation] and twice smaller, $f_M \approx f_P/2$, frequency [half frequency (HF) modulation]. Our simulations show that for the standard and SH modulation the locking regions grow almost linearly with the modulation amplitude a and have nearly the same width. In contrast to that, the HF modulation provides a smaller but strongly nonlinear locking region rapidly increasing with the increase of the modulation amplitude. In Section 3 we perform an asymptotic analysis of model equations and obtain estimates for the locking range width at small modulation amplitudes. We demonstrate that these estimates are valid at moderate and even large modulation amplitudes not only for standard, but also for SH hybrid mode-locking and analyze an impact of different laser parameters on the locking range width. In Section 4 we discuss the experimentally observed asymmetry of the locking regions (see, e.g., Ref. [7]). We show that this asymmetry is related to the dependence of the ML pulse repetition frequency on the modulation amplitude. Finally, in Section 5 we provide experimental evidence of HF modulation hybrid mode-locking in a 20 GHz quantum dot laser. Concluding remarks are presented in Section 6.

2   Simulation of hybrid mode locking

Following [10, 11, 12], we simulate the dynamics of two section ML semiconductor lasers using a dimensionless system of delay differential equations describing unidirectional lasing in a ML ring laser [see Fig. 1(a)].

2.1 Theoretical model

Our mathematical model governs the time evolution of the complex optical field amplitude $A(t)$ at the entrance of the absorber section [see Fig. 1(a)], as well as saturable gain and absorption functions $G(t)$ and $Q(t)$ in the gain and SA parts of the device, respectively:

$$\frac{1}{\gamma}\frac{dA}{dt} = -A + \sqrt{\kappa}e^{\frac{(1-i\alpha_g)G(t-1)-(1-i\alpha_q)Q(t-1)}{2}}A(t-1), \tag{1}$$

$$\frac{dG}{dt} = g_0 - \gamma_g G - e^{-Q}\left(e^G - 1\right)|A|^2; \tag{2}$$

$$\frac{dQ}{dt} = \gamma_q(1+aF(t))(q_0 - Q) - s\left(1 - e^{-Q}\right)|A|^2. \tag{3}$$

By scaling of the time variable, the cold cavity field round-trip time in the device is set to 1, which is also the delay time in the field equation (1). Typical values and a short description of other model parameters are given in Table 1. For more details about the model and its derivation see Refs. [10, 11, 12, 13].

Table 1: Typical parameter values used in simulations

spectral filtering parameter	γ	37.5
non-resonant field losses per cavity round-trip	κ	0.3
linewidth enhancement factor in the gain section	α_g	0
linewidth enhancement factor in the SA	α_q	0
pump parameter	g_0	1.25
unsaturated absorption	q_0	2
gain relaxation rate	γ_g	0.025
SA relaxation rate	γ_q	2.5
ratio of gain/absorber saturation intensities	s	10

In standard hybrid mode-locking the reverse bias applied to the SA section is modulated with a period close to the cavity round trip time. In general, such kind of modulation can affect different laser characteristics. Here, following Refs. [19, 13], we use an approximation, which assumes that the only laser parameter affected by the reverse bias modulation is the absorber relaxation rate γ_q. Therefore in the model equation (3) this rate is multiplied by the factor $1 + aF(t)$, where the function F represents a periodic voltage modulation (VM) with the frequency f_M and the modulation amplitude a.

2.2 Locking regions in a parameter plane

In this subsection we present the results of numerical calculations of the domains of stable hybrid mode-locking where the pulse repetition frequency is locked to the frequency of the external modulation.

First, we performed direct numerical integration of the model equations (1)-(3) with parameters defined in Table 1 and zero amplitude of the VM ($a = 0$). The obtained periodic passive mode locking pulsations had a repetition frequency $f_P \approx 0.9723$.

3

Next, we considered the case of harmonic modulation of the SA reverse bias,

$$F = F_0(t) = \cos\left(2\pi f_M t\right), \tag{4}$$

with the frequency $f_M = f_P + \delta f$, where δf is a small frequency detuning. The width of the locking range at fixed modulation amplitude $a > 0$ was calculated using the following procedure. For each value of the frequency detuning $\delta f_k = k\Delta$ ($k = -M, ..., N$) from the interval $[-M\Delta, N\Delta]$ we performed a long term numerical integration of the model equations (3000 time units) taking the solution calculated at the previous grid point δf_{k-1} as an initial condition. The obtained trajectory was characterized during the last 200 time units of the integration interval.
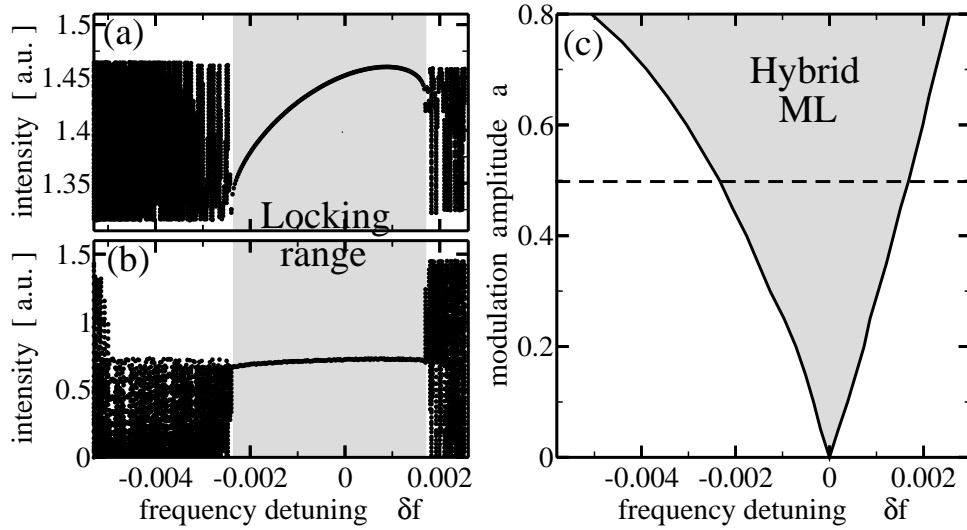

Figure 2: Numerical estimate of the locking range of a hybrid ML laser. (a) Local maxima of the intensity timetrace and (b) $1/f_M$-periodic stroboscopic map points of emitted field intensity time trace at fixed modulation amplitude $a = 0.5$. In the locking range (gray) all ML pulses have the same peak intensity. (c) Locking tongue in the plane of two parameters: frequency detuning δf and modulation amplitude a. Other parameter values are as in Table 1.

The results obtained using this continuation procedure are summarized in Fig. 2(a,b). Panel (a) shows local maxima of the emitted field intensity time trace during the last 200 time units of the integration interval for values of frequency detuning within the interval $-0.006 < \delta f < 0.003$. At sufficiently small $|\delta f|$ locking of the pulse repetition frequency to the frequency of the external modulation f_M is observed. The resulting hybrid mode-locking regime is strictly $1/f_M$ - periodic and all the recorded field maxima at a fixed value of δf have the same value. For frequency detuning outside the locking interval, both frequencies f_M and f_P can be recognized in the simulated irregular or quasi-periodic dynamical regimes. As a consequence, the time-separation between, and the value of, the field intensity maxima varies; multiple intensity peak values are plotted at corresponding frequency detuning δf.

In panel (b) of the same figure, the optical field component of the stroboscopic map for each δf is presented. Here, for each considered δf, we have collected the field intensities separated

4

from each other in time by the interval $1/f_M$. Once locking is achieved and the period of the field intensity time trace becomes equal to $1/f_M$, all stroboscopic map points have the same value. Otherwise, multiple values of this map at a given δf are observed.

Both diagrams in Fig. 2(a,b) were used for estimates of the locking interval (locking range) boundaries, where hybrid mode-locking gains or looses its stability. The dual characterization of the simulated finite time traces during the data post-processing procedure allows us a better characterization of the computed regimes at the locking range boundaries.

By estimating the locking range at different values of the modulation amplitude a we obtain the domain of hybrid ML (the locking tongue) in the plane of two parameters, the modulation frequency detuning and the modulation amplitude, see Fig. 2(c). It can be seen that the locking range grows almost linearly with the modulation amplitude a. Noteworthy that for the parameter values of Fig. 2(c) the locking domain is nearly symmetric with respect to zero frequency detuning, $\delta f = 0$.

2.3 Second-harmonic and half frequency modulations

In this subsection we consider the cases when the external modulation frequency f_M is close either to the second harmonic of the frequency f_P, i.e., $\delta f = f_M/2 - f_P \approx 0$, or to the first subharmonic of this frequency, $\delta f = 2f_M - f_P \approx 0$. We show that in both these cases the pulse repetition frequency can be synchronized with the external modulation. Typical examples of the standard, SH, and HF hybrid ML states are shown in panels (a), (b) and (c) of Fig. 3, respectively.
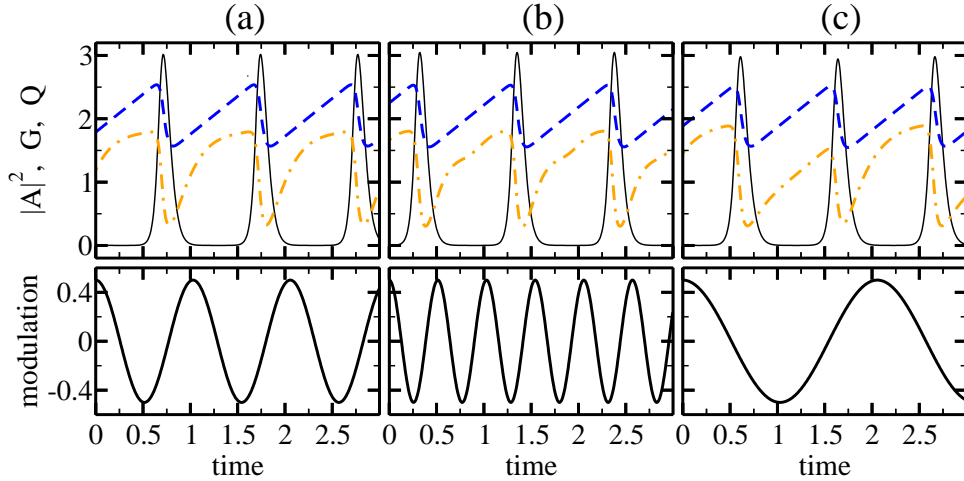

Figure 3: Hybrid ML states for modulation amplitude $a = 0.5$ and (a): $f_M = 0.9725 \approx f_P$. (b): $f_M = 1.945 \approx 2f_P$, and (c): $f_M = 0.48625 \approx f_P/2$. Other parameter values are as in Table 1. Black solid, dashed, and dash-dotted curves in the upper panels represent the field intensity $|A(t)|^2$, gain $G(t)$, and absorption $Q(t)$, respectively. Solid curve in the lower panels represents the time dependence of the modulation function $F(t)$ (4).

In all the cases shown in Fig. 3 the frequency detuning δf is small and the pulse repetition

frequency is close (or equal) to the frequency f_P of the passive mode locking. In the case of standard (panel (a)) and SH (panel (b)) modulation the period of the ML solution is close to the pulse repetition period $1/f_P$ of the free running laser. Note that the SH modulation function $F(t)$ makes exactly two modulation cycles within this period, see solid curve in the lower panel of Fig. 3(b). In contrast to this, in the case of HF modulation, the exact period of the hybrid ML solution is approximately twice larger, $1/f_M \approx 2/f_P$, see Fig. 3(c). According to this figure, each period $1/f_M$ contains a pair of distinct saturation cycles of $Q(t)$ (the dashed-dotted curve in the same panel) and only slightly different pulses of $|A(t)|^2$ or cycles of $G(t)$. This means that two consequent ML pulses generated by means of HF modulation technique are slightly different and this difference increases with the VM amplitude.
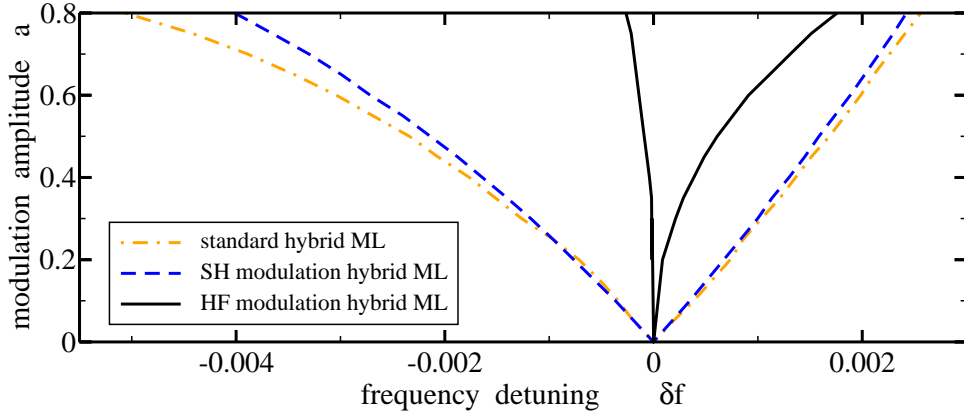

Figure 4: Domains of hybrid mode-locking in the plane of two parameters: frequency detuning and modulation amplitude. Dashed-dotted, dashed, and solid curves represent boundaries of standard, SH, and HF hybrid mode-locking with the pulse repetition frequency f_M, $f_M/2$, and $2f_M$, respectively. Other parameter values are as in Table 1.

Fig. 4 presents the domains of hybrid mode-locking (locking tongues) in the plane of two parameters: frequency detuning and modulation amplitude, for all the three cases discussed above. While the standard and the SH modulation hybrid mode-locking tongues are overlapping and nearly symmetric with respect to $\delta f = 0$, the HF modulation hybrid ML is located within a significantly smaller and strongly asymmetric domain. Moreover, the numerically estimated boundaries of the locking tongue are strongly nonlinear, which makes it difficult to obtain a satisfactory numerical estimate of too narrow locking ranges at small modulation amplitudes a. Such nonlinear dependence of the locking range on the modulation amplitude is typical of the subharmonic resonance 1:2 [16].

3   Asymptotic analysis

Here, using a perturbative approach, we derive an analytical expression for the locking range δf_{LR} in the case of a weak harmonic modulation of the absorber relaxation rate with the frequency, $\delta f \approx 0$.

6

3.1 Estimate of the locking domains

For modulation amplitude $a = 0$ (i.e., modulation function $F \equiv 0$), the model (1)-(4) has a fundamental ML solution

$$A(t) = A_0(t)e^{i\Omega t}, \quad G(t) = G_0(t), \quad Q(t) = Q_0(t), \tag{5}$$

where $A_0(t)$, $G_0(t)$, and $Q_0(t)$ are periodic functions with the period $T_0 = 1/f_P$ close to 1 and the value of Ω depends on the linewidth enhancement factors in the gain and absorber sections, α_g and α_q. Linear stability properties of this solution can be analyzed by substituting a slightly perturbed solution $A(t) = \left[A_0(t) + \delta\psi_1(t)e^{\lambda t} + i\delta\psi_2(t)e^{\lambda t} \right] e^{i\Omega t}$, $G(t) = G_0(t) + \delta\psi_3(t)e^{\lambda t}$, and $Q(t) = Q_0(t) + \delta\psi_4(t)e^{\lambda t}$ into this system. In the linear approximation, the real perturbation vector $\delta\psi(t) = [\delta\psi_1, \delta\psi_2, \delta\psi_3, \delta\psi_4]^T$, where the superscript T denotes transposition, satisfies the equation

$$-\frac{d}{dt}\delta\psi + \mathcal{G}_\psi(t)\delta\psi + \mathcal{H}_\psi(t-1)\delta\psi(t-1)e^{-\lambda} = \lambda\delta\psi, \tag{6}$$

where the Jacobian matrices $\mathcal{G}_\psi$ and $\mathcal{H}_\psi$ are defined in the Appendix. Below we will assume that the unperturbed solution (5) is linearly stable, which means that the real parts of all the eigenvalues λ are negative, except for two zero eigenvalues $\lambda = 0$ associated with the phase shift and time shift symmetries of Eqs. (1)-(4) with $a = 0$. The corresponding periodic eigenfunctions (neutral modes) are $\chi_\varphi(t) = (-\Im A_0, \Re A_0, 0, 0)^T$ and $\chi_\theta = \frac{d}{dt}\psi_0$ respectively. Here $\psi_0 = (\Re A_0, \Im A_0, G_0, Q_0)^T$, The adjoint neutral vector-eigenfunctions $\chi_\varphi^\dagger(t)$ and $\chi_\theta^\dagger(t)$ are defined as periodic solutions of the adjoint linear problem with zero eigenvalue λ:

$$\frac{d}{dt}\delta\psi^\dagger + \mathcal{G}_\psi^T(t)\delta\psi^\dagger + \mathcal{H}_\psi^T(t)\delta\psi^\dagger(t+1) = 0. \tag{7}$$

These modes satisfy the biorthogonality conditions

$$\langle \chi_j, \chi_k^\dagger \rangle := \int_0^{T_0} \sum_{s=1}^4 \chi_{js}(t')\chi_{ks}^\dagger(t')dt' = \delta_{kj}, \tag{8}$$

where $j, k = \varphi, \theta$, and δ_{kj} is the Kronecker symbol. To calculate the adjoint neutral modes we solve Eq. (7) numerically in reverse time with two linearly independent initial conditions $\chi_1^\dagger(t)$ and $\chi_2^\dagger(t)$ at $0 \leq t \leq 1$. The functions $\chi_\varphi^\dagger$ and $\chi_\theta^\dagger$ then are found as linear combinations of two periodic linearly independent solutions of Eqs. (8).. In the case $\alpha_g = \alpha_q = \Omega = 0$, the two adjoint neutral modes can be found separately by solving two decoupled sets of equations [13, 17].

For nonzero modulation amplitudes a the time shift invariance of the model equations is broken, which can lead to a synchronization of the pulse repetition frequency f_P to the external modulation frequency f_M. When the frequency detuning $\delta f = f_M - f_P$ is sufficiently small, the hybrid mode locking with the pulse repetition frequency f_M can appear. We use perturbation analysis to estimate the width of the locking range δf_{LR} at small modulation amplitudes $a \ll 1$. To this end we look for a solution of Eqs. (1)-(4) in the form

$$A(t) = [A_0(t + \theta) + \delta A_1 + i\delta A_2] e^{i\Omega t + i\varphi}, \tag{9}$$

$$G(t) = G_0(t + \theta) + \delta G, \quad Q(t) = Q_0(t + \theta) + \delta Q, \tag{10}$$

where θ and φ are slowly varying functions of time, $\frac{d\theta}{dt} = \mathcal{O}(a)$ and $\frac{d\varphi}{dt} = \mathcal{O}(a)$. In the locked state, when the pulse repetition frequency coincides with f_M, we have $f_P(1 + \frac{d\theta}{dt}) = f_M$, time independent $\frac{d\theta}{dt} = \delta f / f_P$, and the phase $\theta(t) = \theta(0) + t\delta f / f_P$. On the other hand, substituting (9) and (10) into Eq. (1)-(4) and collecting first order terms in the small parameter a, we obtain an inhomogeneous linear equation for the real vector $\delta\eta = (\delta A_1, \delta A_2, \delta G, \delta Q)^T = \mathcal{O}(a)$:

$$\frac{d}{dt}\delta\eta - \mathcal{G}_\psi(t)\delta\eta - \mathcal{H}_\psi(t-1)\delta\eta(t-1) = \mathcal{A}(t), \tag{11}$$

where $\mathcal{A}(t) = \mathcal{O}(a)$ is given in the Appendix. According to the Fredholm alternative, this equation is solvable provided its inhomogeneous part is orthogonal to the adjoint neutral modes $\chi_\theta^\dagger$ and $\chi_\varphi^\dagger$. This criterion leads to a pair of equations which are linear with respect to the derivatives $\frac{d\theta}{dt}$ and $\frac{d\varphi}{dt}$. By eliminating $\frac{d\varphi}{dt}$, we obtain the following single differential equation for θ:

$$\frac{d\theta}{dt} = a \sum_{j=\phi,\theta} c_j \int_0^{T_0} [q_0 - Q_0(t')]F(t'-\theta)\chi_{j4}^\dagger(t')dt', \tag{12}$$

where the coefficients c_ϕ and c_θ are defined in Appendix. For modulation function (4), we assume that $|\delta f| \ll f_P$ and neglect the term $\theta\delta f$ in the argument of F. The resulting condition for the existence of the $1/f_M$-periodic function $\hat{\psi}$ reads as

$$\delta f = acf_P \cos[2\pi f_P\theta(0) - \zeta], \tag{13}$$

with the coefficients c and ζ defined in Appendix. This condition can be satisfied only for $|\delta f| \leq acf_P$, which, finally, gives us the estimate for the width of the locking range:

$$\delta f_{LR} = 2acf_P. \tag{14}$$

In Fig. 5(a) the locking range width obtained using Eq. (14) is compared to that calculated by direct numerical integration of Eqs. (1)-(4). It is seen that the asymptotic relation (14) gives a good approximation of δ_{LR} even for relatively large modulation amplitudes a.

Similar techniques can be used for estimating the locking range in the case of SH modulation considered in the previous section, but not for HF modulation, since for the latter type of modulation the dependence of the locking range width on the modulation amplitude is nonlinear at small a, $\delta f_{LR} = \mathcal{O}(a^2)$.

For SH modulation $\delta f = f_M/2 - f_P \ll 1$ and the period of the locked solution $2/f_M$ is close to T_0. Thus, the only difference in derivation of the locking estimate coefficient c in Eq. (14) occurs due to a different expression for the function $F(t - \theta) \approx \cos\{4\pi f_P[t - \theta(0)]\}$ in Eq. (12). Like in the standard hybrid mode-locking case, the resulting estimate can be also applied for relatively large a, see Fig. 5(b).

3.2 Parameter study

In Eq. (14) the ratio $\delta f_{LR}/a$ characterizes the ability of the mode-locking regime to be locked to a reverse bias modulation. The dependence of this ratio on parameters of Eqs. (1)-(3) is
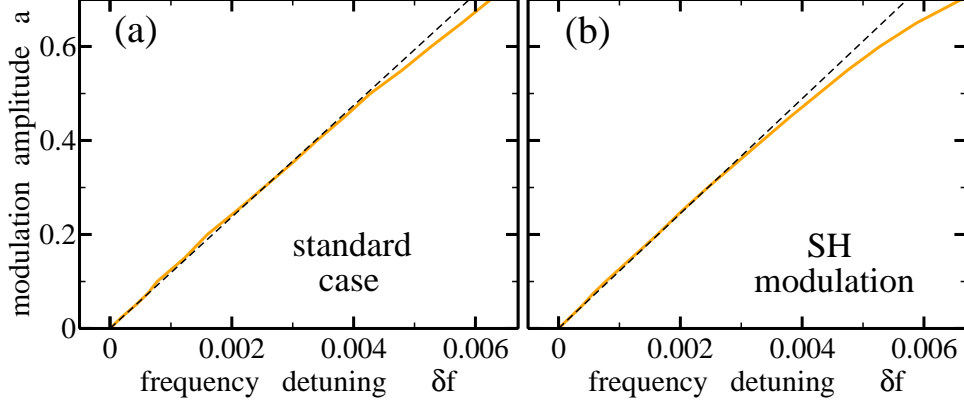
Figure 5: Estimation of δ_{LR} of the hybrid ML regions in dependence on the modulation amplitude a for (a): standard and (b): SH hybrid mode-locking. Thick solid curves: numerical integration of Eqs. (1)-(4). Thin dashed lines: asymptotic estimates for $a \ll 1$. $\alpha_g = 1.7$, $\alpha_q = 1$, while other parameters are as in Table 1.

illustrated in Figs. 6 and 7, where different curves on the same plot represent different values of the gain parameter g_0, which corresponds to the injection current applied to the gain section. In particular, it follows from the data shown in Fig. 6(a) that for sufficiently large linear gains g_0 the locking range is inversely proportional to the square of the spectral filtering widths, $\delta f_{LR} \propto \gamma^{-2}$. Figure 6(b) illustrates the dependence of $\delta f_{LR}/a$ on the saturation parameter s. It is seen that with the increase of this parameter the locking range width decreases. A similar decrease of the locking range takes place with the increase of the linear attenuation factor κ, i.e., with the decrease of linear non-resonant losses per cavity round trip, see Fig. 6(c). Fig. 6(d) illustrates the increase of locking range with the absorber relaxation rate γ_q.
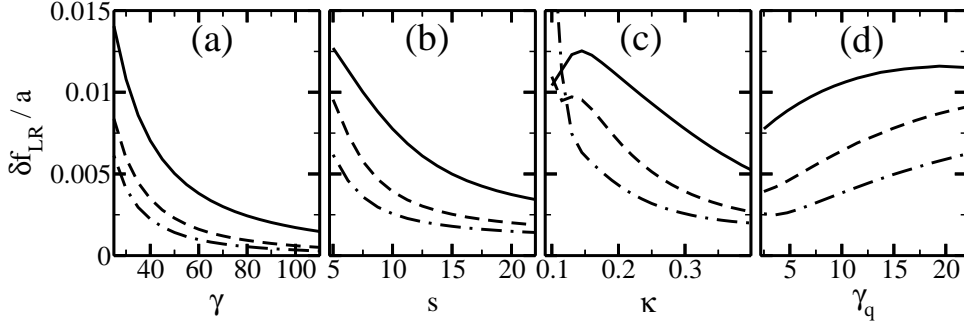

Figure 6: Dependence of the ratio $\delta f_{LR}/a$ characterizing the locking tongue width on parameters of the model equations (1)-(3). Solid, dashed, and dash-dotted lines correspond to $g_0 = 1.25$, $g_0 = 2.0$, and $g_0 = 2.75$, respectively. Other parameter values are as in Table 1.

Now let us consider the dependence of the locking range width on the linewidth enhancement factors in the gain and absorber sections. When these factors are sufficiently large the ML regime usually degrades. To avoid this degradation, we consider a laser operation not far away from the lasing threshold for relatively small value of the linear gain parameter, $g_0 = 1.25$. As it is seen from Fig. 7(a), the locking range increases with simultaneous increase of the two
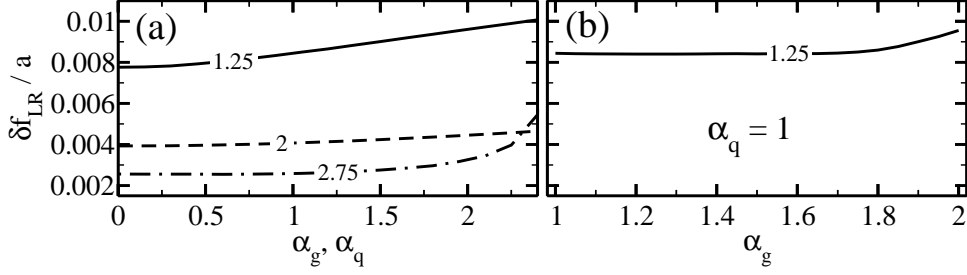
Figure 7: Dependence of the ratio $\delta f_{LR}/a$ on the linewidth enhancement factors $\alpha_g = \alpha_q$ (a) and α_g with fixed $\alpha_q = 1$ (b). Solid, dashed, and dash-dotted lines correspond to $g_0 = 1.25$, $g_0 = 2.0$, and $g_0 = 2.75$, respectively. Other parameter values are as in Table 1.

linewidth enhancement factors, $\alpha_g = \alpha_q$. For fixed $\alpha_q = 1$ the locking range remains almost constant with the increase of α_g up to $\alpha_g \leq 1.7$, and starts to increase at higher values of the linewidth enhancement factor in the gain section, $1.7 \leq \alpha_g \leq 2$ (see Fig. 7(b)). At $\alpha_g \geq 2$ we observed a degradation of the ML regime for the chosen parameter values. Finally, we have found that for nonzero α-factors, $\alpha_q = 1$, $\alpha_g = 1.7$, and $g_0 = 1.25$, the dependencies of the locking range width on the laser parameters are qualitatively similar to those shown in Fig. 6 corresponding to $\alpha_g = \alpha_q = 0$.

4 Asymmetry of the hybrid ML regions

In this section we discuss reasons for the locking range asymmetry, which was observed experimentally in hybrid ML lasers [8, 9]. Up to now we have considered the harmonic modulation function $F = F_0$ defined in Eq. (4). In this case, at small modulation amplitudes a, the locking tongue was nearly symmetric with respect to zero detuning $\delta f = f_M - f_P = 0$ (see, e.g., dash-dotted line in Fig. 4). This fact is in agreement with the locking condition (13), where minimal and maximal values of δf, corresponding to lower and upper locking range boundary, have the same absolute value and differ only by their signs.

Although under experimental conditions the absorber voltage modulation is harmonic, its impact on the modulation of the saturable absorber relaxation rate γ_q is, in general, nonlinear: see, e.g., Ref. [19], where an exponential dependence of the carrier relaxation time on the voltage applied to the absorber section was suggested. Hence, a realistic profile of the function F can be significantly different from the harmonic one. Let us consider the modulation functions

$$F = F_{\pm}(t) = \pm \left(1 - 2\cos^{10}(\pi f_M t) \right), \tag{15}$$

schematically depicted in Fig. 8. Similarly to the harmonic modulation case (4), the period, the maximal value, and the minimal value of these functions are given by $1/f_M$, 1, and -1, respectively. However, unlike the case of harmonic modulation, the time-averaged values $\langle F_{\pm} \rangle = f_M \int_0^{1/f_M} F_{\pm}(t)dt = \pm\frac{65}{128}$ of the two functions defined by Eq. (8) are not equal to zero. Therefore, the time averaged absorber relaxation rate $\langle \gamma_q(1 + aF_{\pm}) \rangle$ depends on the amplitude a.

Locking tongues for the modulation functions (15) are presented in Fig. 8. The inset in this
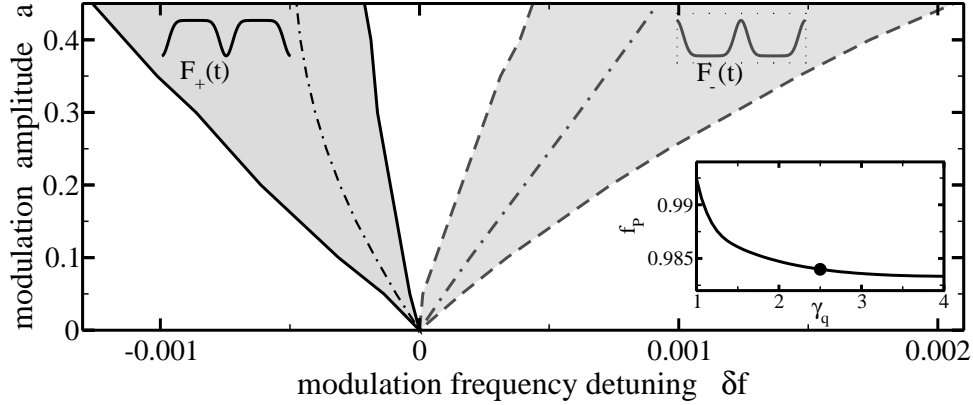
Figure 8: Domains of hybrid mode-locking for pulsed modulation profiles $F_\pm$ defined by Eq. (15). These profiles are shown inside the corresponding tongues. Dash-dotted curves in the middle of the locking tongues represent frequency shifts $\delta f_P(a)$ defined by Eq. (16). Inset shows the dependence of the pulse repetition frequency f_P of the free running laser on the absorber relaxation rate γ_q. Thick bullet indicates the value of γ_q used in numerical simulations of the locking tongues and the corresponding value of the pulse repetition rate $f_P(\gamma_q)$ of the free running laser. $g_0 = 2.5$. Other parameter values are as in Table 1.

figure shows the dependence of the pulse repetition frequency of the free running ML laser on the SA relaxation rate, $f_P = f_P(\gamma_q)$. It is seen that the increase of the relaxation rate, which corresponds to an increase of applied modulation amplitude a, results in a decrease of the ML frequency f_P. Dash-dotted lines in Fig. 8 show the dependence of the detuning δf_P of the pulse repetition frequency evaluated at the mean value of the absorber relaxation rate on the modulation amplitude a:

$$\delta f_P^\pm(a) \stackrel{def}{=} f_P\left(\langle\gamma_q(1 + aF_\pm(t))\rangle\right) - f_P\left(\gamma_q\right). \tag{16}$$

We see that with the increase of the amplitude a the central frequencies of the two locking ranges obtained for the modulation functions $F_\pm(t)$ remain very close to the dash-dotted lines defined by relation (16). Therefore, we can conclude that the asymmetry of the locking tongues in Fig. 8 is related to the dependence of the pulse repetition frequency on the amplitude a of VM in the absorber section.

5   Experiments

Here we present the first experimental evidence subharmonic (HF) voltage modulation (VM) hybrid mode-locking in a quantum-dot laser. The structure is grown by molecular beam epitaxy on an n^+-doped GaAs substrate. The active region contains 10 layers of InAs QDs in a 'dot-in-a-well' structure in order to shift the emission wavelength to 1310 nm. The wafer is processed using dry etching techniques yielding a 4μm wide waveguide ridge. For high frequency applications BCB interlayers are used. The 1985 μm long laser chip consists of a 285μm long reversely biased saturable absorber section and a 1680μm forward biased gain section which are separated by a dry etched 20μm gap. While the saturable absorber facet is high-reflection (99%)

coated, the gain section facet is left as cleaved. The electrical spectra have been measured using a 50 GHz electrical spectrum analyzer in combination with a high-speed photodetector having a bandwidth larger than 50 GHz.
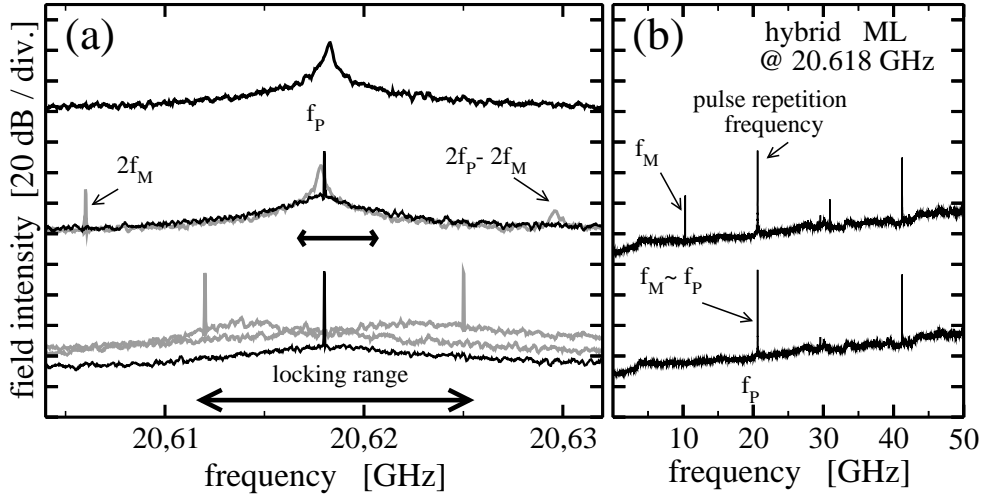

Figure 9: Measured RF spectra of passively and hybrid ML laser. Gain section bias current, SA voltage, and full amplitude of VM are 100 mA, -3 V, and 3.2 V, respectively. (a) top: passive ML; middle: HFVM hybrid ML (black) and non-synchronized state (gray); bottom: standard hybrid ML in the middle (black) and at the boundaries (gray) of the locking range. Thick horizontal arrows indicate locking ranges in the classical and HFVM hybrid ML cases. (b): large frequency span overview of the standard (above) and HFVM (below) hybrid ML spectra shown by corresponding black curves in panel (a).

In the absence of external VM, after selecting appropriate gain section injection current and absorber voltage, the laser demonstrated stable passive ML pulsations with $f_P \sim 20.62$ GHz pulse repetition frequency corresponding to the inverse round-trip time of the laser radiation in the cavity, see upper RF spectrum in panel (a) of Fig. 9. As it is typical for passive ML, the RF spectral line was relatively broad, indicating a significant time jitter of the emitted pulses

In a laser with modulated absorber bias the full amplitude of the modulated voltage was set to 3.2 V (14 dBm), which was the upper limit available in our experiments. First we consider the case when the frequency f_M of the external VM applied to the absorber section is close to f_P. By tuning properly f_M hybrid ML was achieved in a certain locking range. This range is indicated by horizontal arrow at the bottom of Fig. 9(a). The RF spectra of the hybrid ML laser are shown in the lower parts of panels (a) and (b) in Fig. 9. The wide span of the RF spectrum (panel (b)) has a spectral peak only at $\sim f_P$ and its second harmonic, and has no low frequency components which are typical for Q-switched ML or irregular ML with modulated amplitudes [18]. The narrow span RF spectra (panel (a)) show a significant improvement of the spectral linewidth, which indicates a considerable reduction of the pulse time jitter. Noteworthy, that the frequency f_P (peak frequency of the upper RF spectrum in panel (a)) is located almost at the center of the estimated locking range. This suggests that in this case the locking tongue is almost symmetric with respect to $f_M = f_P$ line in the VM frequency / VM amplitude plane.

12

Next, we took f_M close to $f_P/2 \approx 10.31$ GHz. As it can be seen from the upper curve of panel (b), in this case the RF spectrum demonstrates peaks at frequencies f_M, f_P, and their higher harmonics. A narrow span of the RF spectrum represented by gray curve in the middle part of panel (a) indicates also the presence of the combination tone $\sim (f_P - 2f_M)$. The middle part of panel (a) gives also an illustration of the synchronization between the VM and the passive ML pulsations. The nonlinear nature of the interaction between optical fields and carriers in the laser cavity together with a nonlinear dependence of laser parameters on the modulation amplitude [19] imply the presence of spectral peaks at higher harmonics of the modulation frequency f_M. In our HF experiments the role of the second harmonic peak at $2f_M$ is similar to that of the spectral peak at f_M in standard hybrid mode-locking. Namely, for sufficiently large detuning between the frequencies $2f_M$ and f_P both these spectral components are present in the RF spectra: see gray curve in the middle part of panel (a). As soon as the frequency separation becomes sufficiently small, the broad spectral peak at f_P locks to the sharp spectral line at $2f_M$ (black curve in the middle part of panel (a)), which implies the appearance of HF hybrid mode-locking. Since the amplitude of the second harmonic of VM at $2f_M$ is smaller then that of the first harmonic at f_M, the locking range in standard hybrid mode-locking is wider than the locking range of a HF hybrid ML laser, see black horizontal arrow below corresponding spectra in panel (a). Furthermore, HF hybrid mode-locking is characterized by a smaller height of the sharp spectral peak [compare black spectra at the middle and at the bottom of panel (a)] and, hence, by a larger pulse time jitter as compared to standard ML. We note also that while the pulse repetition frequency remains close to f_P, strictly speaking, the period of the laser intensity time trace in the HF hybrid ML state is approximately twice larger then that in a passively ML laser, $1/f_M \approx 2/f_P$. This means that two consequent ML pulses are slightly different (see also numerical results presented in Fig. 3(b)). An increase of the VM amplitude could lead to a larger locking range, and at the same time to a growth of the difference between a pair of subsequent pulses.

6 Conclusions

In conclusion, we studied hybrid mode-locking in a two section edge-emitting semiconductor laser. Dependence of the locking range on the laser parameters has been studied numerically and analytically. The voltage modulation in the SA section of the device was represented by modulated carrier relaxation rate in this section. It has been demonstrated numerically that the locking range increases almost linearly with the increase of the modulation amplitude. We have shown that the asymmetry of the locking range is related to the dependence of the averaged absorber relaxation rate on the modulation amplitude a, which has an impact on the frequency of the passive ML pulsations.

Analytical estimates of the the locking range width have been obtained using an asymptotic approach. According to these estimates the locking range in hybrid ML lasers increases with the decrease of the spectral filtering bandwidth γ.

Locking tongues, where the pulse repetition rate was synchronized to the frequency of the external modulation, were found theoretically for modulation frequencies f_M close to f_P (standard hybrid mode-locking), $2f_P$ (SH hybrid mode-locking), and $f_P/2$ (HF hybrid mode-locking).

Unlike standard and SH hybrid mode-locking, for which the dependence of the locking range width on the modulation amplitude a was almost linear, the locking range in HF mode-locking, corresponding to a resonance $1 : 2$, was smaller and increased nonlinearly with a. Finally, we provided an experimental evidence of such kind of HF hybrid mode-locking in a 20 GHz quantum-dot laser.

Appendix

Here we list the formulas used in the derivation of the locking range width δf_{LR} in Section 3.

The real 4×4 Jacobian matrices $\mathcal{G}$ and $\mathcal{H}$ in Eq. (6) are given by

$$\mathcal{G}_\psi(t) = \left.\frac{\partial \mathcal{G}}{\partial \psi}\right|_{\psi=\psi_0(t),a=0}, \quad \mathcal{H}_\psi(t) = \left.\frac{\partial \mathcal{H}}{\partial \psi}\right|_{\psi=\psi_0(t)},$$

where $\psi_0(t) = [\Re A_0, \Im A_0, G_0, Q_0]^T$,

$$\mathcal{G} = \begin{pmatrix} -\gamma\psi_1 + \Omega\psi_2 \\ -\Omega\psi_1 - \gamma\psi_2 \\ g_0 - \gamma_g\psi_3 - e^{-\psi_4}(e^{\psi_3}-1)\left(\psi_1^2 + \psi_2^2\right) \\ \gamma_q(1+aF)(q_0-\psi_4) - s(1-e^{-\psi_4})\left(\psi_1^2 + \psi_2^2\right) \end{pmatrix},$$

and

$$\mathcal{H} = (r_1\psi_1 - r_2\psi_2, r_2\psi_1 + r_1\psi_2, 0, 0)^T$$

with $r_1 = \Re r$, $r_2 = \Im r$, $r = \gamma\sqrt{\kappa}e^{\frac{(1-i\alpha_g)\psi_3-(1-i\alpha_q)\psi_4}{2}-i\Omega}$.

The right hand side of Eq. (6) is given by

$$\begin{aligned} \mathcal{A}(t) &= [0, 0, 0, a\gamma_q(q_0 - \psi_{04}(t))F(t-\theta)]^T \\ &- \frac{d\varphi}{dt}\mathcal{S}\{\psi_0(t) + \mathcal{H}\left(\psi_0(t-1)\right)\} \\ &- \frac{d\theta}{dt}\left[\frac{d\psi_0(t)}{dt} + \mathcal{H}_\psi(t-1)\frac{d\psi_0(t-1)}{dt}\right], \end{aligned}$$

where $\mathcal{S} = \begin{pmatrix} \hat{\sigma} & \hat{0} \\ \hat{0} & \hat{0} \end{pmatrix}$, $\hat{\sigma} = \begin{pmatrix} 0 & -1 \\ 1 & 0 \end{pmatrix}$, and $\hat{0}$ is the 2x2 zero matrix. Orthogonality of the right hand side $\mathcal{A}$ of Eq. (11) and the neutral modes $\chi_j^\dagger$, $j = \phi, \theta$ together with the expressions for these modes give us

$$\begin{aligned} &a\gamma_q \int_0^{T_0} \left[q_0 - \psi_{04}(t)\right] F(t-\theta)\chi_{j4}^\dagger dt \\ &= (c_{j1} + \delta_{\theta j})\frac{d\theta}{dt} + [c_{j2} + (1+\gamma)\delta_{\phi j}]\frac{d\varphi}{dt}, \end{aligned} \tag{17}$$

with

$$\begin{aligned} c_{j1} &= \langle \mathcal{H}_\psi(t)\frac{d}{dt}\psi_0(t), \chi_j^\dagger(t+1)\rangle = \int_0^{T_0} \frac{d}{dt}\left(\frac{d\psi_{01}}{dt} + \gamma\psi_{01}\right. \\ &\left. -\Omega\psi_{02}\right)\chi_{j1}^\dagger dt + \int_0^{T_0} \frac{d}{dt}\left(\frac{d\psi_{02}}{dt} + \Omega\psi_{01} + \gamma\psi_{02}\right)\chi_{j2}^\dagger dt, \\ c_{j2} &= \langle \mathcal{S}\{\mathcal{H}(\psi_0(t-1)) - \gamma\psi_0(t)\}, \chi_j^\dagger(t)\rangle \\ &= \int_0^{T_0} \left[-\left(\frac{d\psi_{02}}{dt} + \Omega\psi_{01}\right)\chi_{j1}^\dagger + \left(\frac{d\psi_{01}}{dt} - \Omega\psi_{02}\right)\chi_{j2}^\dagger\right] dt. \end{aligned}$$

14

Eliminating $\frac{d\phi}{dt}$ from the system of two equations (17), we obtain Eq. (12) with the coefficients

$$c_j = \gamma_q \frac{c_{\theta 2}\delta_{\phi j} - (1 + \gamma + c_{\phi 2})\delta_{\theta j}}{c_{\theta 2}c_{\phi 1} - (1 + \gamma + c_{\phi 2})(1 + c_{\theta 1})}, \quad j = \phi, \theta.$$

Finally, for the modulation function (4), the coefficients for the locking condition (13) are given by

$$
\begin{aligned}
c &= \sqrt{(c_\phi c_{\phi c} + c_\theta c_{\theta c})^2 + (c_\phi c_{\phi s} + c_\theta c_{\theta s})^2}, \\
\zeta &= \arcsin\left((c_\phi c_{\phi s} + c_\theta c_{\theta s})/c\right), \\
c_{jc} &= \int_0^{T_0} \chi_{j4}^\dagger (q_0 - Q_0(t)) \cos\left(2\pi f_P t\right) dt, \ j \in \{\phi, \theta\}, \\
c_{js} &= \int_0^{T_0} \chi_{j4}^\dagger (q_0 - Q_0(t)) \sin\left(2\pi f_P t\right) dt, \ j \in \{\phi, \theta\}.
\end{aligned}
$$

References

[1] D. Bimberg, M. Grudmann and N. N. Ledentsov, *Quantum dot heterostructures*. J. Wiley, 1999.

[2] D. Bimberg, Quantum dot based nanophotonics and nanoelectronics, *Electron. Lett.* **44**, pp. 168–171, 2008.

[3] D. Bimberg, Quantum dots for lasers, amplifiers and computing *J. Phys. D* **38**, pp. 2055–2058, 2005.

[4] M. Kuntz *et al.*, Direct modulation and mode locking of 1.3 μm quantum dot lasers. New J. Phys. **6**, 181, 2004.

[5] R. Kaiser and B. Hüttl, "Monolithic 40-GHz Mode-Locked MQW DBR Lasers for High-Speed Optical Communication Systems," IEEE Journal of Selected Topics in Quantum Electronics, **13**, 125-135 (2007).

[6] M. Kuntz *et al.*, "High speed mode-locked quantum dot lasers and optical amplifiers," *Proceedings of the IEEE* **95**, pp. 1767–1778, 2007.

[7] M.G. Thompson *et al.*, "InGaAs quantum dot mode-locked laser diodes," *IEEE J. Sel. Top. Quant.* **15**, pp. 661–672, 2009.

[8] G. Fiol *et al.*, "Hybrid mode-locking in a 40 GHz monolithic quantum dot laser," *Appl. Phys. Lett* **96**, p. 011104, 2010.

[9] H. Schmeckebier, G. Fiol, C. Meuer, D. Arsenijević, and D. Bimberg, "Complete pulse characterization of quantum-dot mode-locked lasers suitable for optical communications up to 160 Gbit/s, Öpt. Express **18**, 3415-3425 (2004).

[10] A.G. Vladimirov, D. Turaev, and G. Kozyreff, "Delay differential equations for mode-locked semiconductor lasers, Öpt. Lett. **29**, 1221-1223, 2004.

[11] A.G. Vladimirov and D. Turaev, Ä new model for a mode-locked semiconductor laser,"Radiophysics and Quantum Electronics, **47**, 769-776 (2004).

[12] A. G. Vladimirov and D. Turaev, "Model for passive mode locking in semiconductor lasers," *Phys. Rev A* **72**(3), p. 033808, 2005.

[13] A. G. Vladimirov *et al.*,"Locking characteristics of a 40-GHz hybrid mode-locked monolithic quantum dot laser," *Proc. of SPIE* **7720**, p. 77200Y, 2010.

[14] E.A. Viktorov, P. Mandel, A.G.Vladimirov, and U. Bandelow, Ä model for mode-locking in quantum dot lasers, Äpplied Physics Letters, **88**, 201102 (2006).

[15] A. G. Vladimirov, U. Bandelow, G. Fiol, D. Arsenijevic, M. Kleinert, D. Bimberg, A. Pimenov, and D. Rachinskii, "Dynamical regimes in a monolithic passively mode-locked quantum dot laser,"JOSA B **27**, 2102-2109 (2010).

[16] V. I. Arnold, Geometrical methods in the theory of ordinary differential equations, (Springer, Berlin, 1983).

[17] N. Rebrova *et al.*,"An optically injected mode locked laser," *Phys. Rev. E* **88**, p. 066202, 2011.

[18] U. Bandelow, M. Radziunas, A. Vladimirov, B. Hüttl, R. Kaiser, "Harmonic mode-locking in monolithic semiconductor lasers: theory, simulations and experiment," *Optical and Quantum Electronics* **38**, pp. 495–512, 2006.

[19] E.A. Viktorov *et al.*, "Recovery time scales in a reversed-biased quantum dot absorber," *Appl. Phys. Lett.* **94**, p. 263502, 2009.